Available online at www.sciencedirect.com
ScienceDirect
Trans. Nonferrous Met. Soc. China 25(2015) 2958−2964
Transactions of Nonferrous Metals Society of China
www.tnmsc.cn

Effect of minor B addition on microstructure and properties of AlCoCrFeNi multi-compenent alloy

Qiu-shi CHEN, Yi-ping LU, Yong DONG, Tong-min WANG, Ting-ju LI

School of Materials Science and Engineering, Dalian University of Technology, Dalian 116024, China

Received 17 November 2014; accepted 25 March 2015

Abstract: The influences of slight amount of B element on the microstructure and properties of $AlCoCrFeNiB_x$ high entropy alloys (x = 0, 0.01,⋯, 0.09 and 0.1, mole fraction) were investigated. The AlCoCrFeNi high entropy alloy exhibits equiaxed grain structures with obvious composition segregation. However, with the addition of B element, the alloys exhibit dendrite structures. Inside the dendrites, spinodal decomposition structure can be clearly observed. With the addition of B element, the crystal structures change from ($B2$ + BCC) to ($B2$ + BCC + FCC) structures, and the hardness firstly increases from HV 486.7 to HV 502.4, then declines to HV 460.7 ($x \geq 0.02$). The compressive fracture strength firstly shows a trend of increasing, and then declining ($x \geq 0.08$). The coercive forces and the specific saturation magnetizations of the alloys decrease as B addition contents increase, the decreasing coercive forces show a better soft magnetic behavior.

Key words: high entropy alloy; B element; microstructure; compressive properties; hardness; magnetic properties

1 Introduction

Conventional alloy-design strategy is mainly based on one or two principal components, while other elements are regarded as minor components to improve the properties [1,2]. Different from the conventional one, a new alloy-design strategy was proposed by CANTOR et al [3] and YEH et al [4], and the alloys were named by high-entropy alloys (HEAs) or multi-principal element alloys. At present, HEAs have become a new research hotspot in the field of materials science [5].

A lot of researches based on the AlCoCrFeNi equiatomic alloy have been done, such as $FeCoNiCrCu_{0.5}Al_x$ [6], $FeNiCoCrAl_3$ [7], FeTiCoNiVCr-MnCuAl [8], $AlCoCrFeNiNb_x$ [9], $AlCoCrFeNiC_x$ [10] and $AlCoCrFeNiV_x$ [11] alloys. However, in these alloy systems, the amounts of additions were mostly above 0.1 in molar ratio. Few researches about HEAs with a small amount of element additions have been studied before. And in this study, B element was selected for the following reasons: firstly, B and other elements have large negative mixing enthalpies (the values of B and Co, B and Cr, B and Fe, B and Ni atomic pairs are −24, −31, −26 and −24 kJ/mol, respectively) [12,13], which leads to the formation of borides, and the borides can improve the compression strength and wear resistance of alloys; secondly, the atomic radius of B element is much smaller than that of other elements, which can result in the diffusion during solidification more easily. And diffusion is a key factor of controlling phase transition [14]. The transition of the morphologies and microstructure is crucial to mechanical properties. Next, a small amount of B element is usually able to refine the grain size [15]. At last, some alloys containing B element may possess good soft magnetic property [16]. Therefore, in this work, the effects of B element addition from 0 to 0.1 in molar fraction on the microstructures and properties of the $AlCoCrFeNiB_x$ HEAs were investigated in detail.

2 Experimental

The HEAs ingots of $AlCoCrFeNiB_x$ (x: mole ratio, x=0, 0.01, ⋯, 0.09 and 0.1, denoted by BM0, BM1, ⋯, BM9 and BM10, respectively) were prepared by vacuum

Foundation item: Projects (51134013, 51104029, 51471044) supported by the National Natural Science Foundation of China; Project supported by the Fundamental Research Funds for the Central Universities, China; Project (LZ2014007) supported by the Key Laboratory of Basic Research Projects of Liaoning Province Department of Education, China; Project (2014028013) supported by the Natural Science Foundation of Liaoning Province, China

Corresponding author: Yi-ping LU; Tel: +86-411-84709400; Fax: +86-411-84708940; E-mail: luyiping@dlut.edu.cn

DOI: 10.1016/S1003-6326(15)63922-X

arc furnace under a Ti-gettered high-purity argon atmosphere. The purity of all the raw materials (Al, Co, Cr, Fe, Ni, B) was above 99.9%. The alloys were flipped and remelted at least five times. The 30 g button ingots were directly solidified in a water-cooled cold copper hearth.

X-ray diffractometer (XRD, Shimadzu XRD−6000) with Cu K_α radiation was used for the phase analysis, with scanning angle ranging from 20° to 100° at a speed of 4 (°)/min. Microstructures, phase compositions and fracture surfaces were observed by using a scanning electron microscope with energy dispersive spectrometry (SEM, Zeiss supra55). The size of the samples for the tests of compressive properties was *d*5 mm × 10 mm. The tests were conducted at a strain rate of 1.0 s^{-1}. The hardness test was conducted through Vickers hardness tester model (MH−60) with 1 kg for 15 s. Five measurements were made for each sample to obtain the averaged experimental data. The magnetization curves were measured with a JDM−13T vibrating sample magnetometer.

3 Results and discussion

3.1 X-ray diffraction analysis

Figure 1 shows the XRD patterns of the $AlCoCrFeNiB_x$ HEAs. When x=0, the alloy exhibits the mixing structures of *B*2 and BCC. That is consistent with previous research results [17]. As the B content increases, the intensity of BCC phase diffraction peaks decreases. In addition, the diffraction peaks of FCC phase appear from BM2 alloy, and the intensity gradually increases with the increase of B content. So, a conclusion can be inferred that the transformation from BCC phase to FCC phase occurs as B content increases.

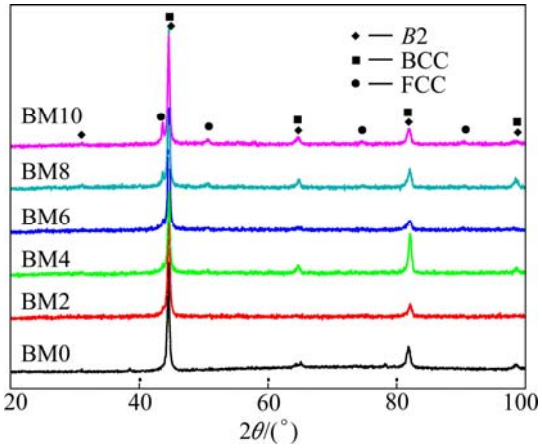

Fig.1 XRD patterns of $AlCoCrFeNiB_x$ HEAs

3.2 Microstructure and characterization

Figures 2 and 3 display the SEM images of the microstructures of the $AlCoCrFeNiB_x$ HEAs. BM0 alloy exhibits typical equiaxed grain morphology, accompanying with obvious intragranular segregation, as shown in Fig. 2(a). The bright segregation area and the dark segregation area are denoted as *A* and *B*, respectively. Typical spiondal decomposition microstructure can be observed in the interior of the grains. According to the previous research, the bright section and the dark section of interconnected microstructure were composed of (Fe, Co, Cr)-rich element and (Al, Ni)-rich element whereas section *A* has a higher amount of Al and Ni than section *B* [18].

With the B element addition, BM1−BM10 alloys all exhibit dendritic morphology as seen in Fig. 2. The atomic radius of B element is far smaller than thoes of Al, Co, Cr, Fe and Ni elements, which may lead to the large

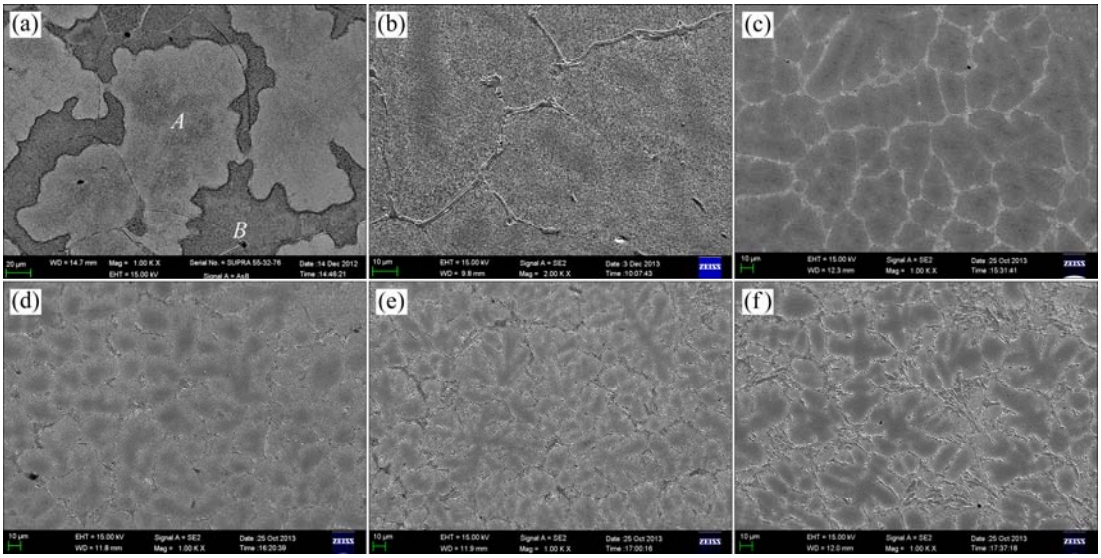

Fig. 2 SEM images of $AlCoCrFeNiB_x$ HEAs in low magnification: (a) BM0; (b) BM2; (c) BM4; (d) BM6; (e) BM8; (f) BM10

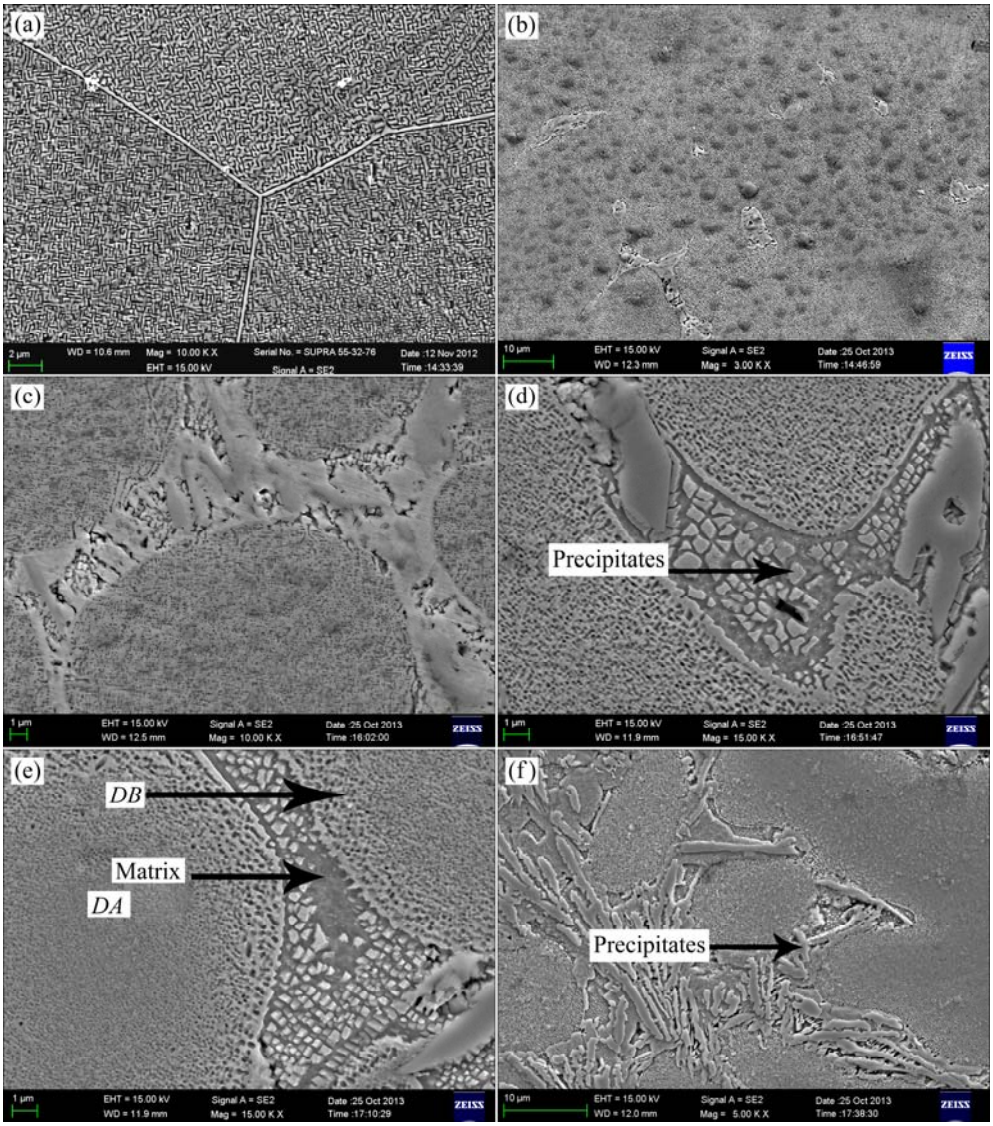

Fig. 3 SEM images of AlCoCrFeNiB$_x$ HEAs in high magnification: (a) BM0; (b) BM2; (c) BM4; (d) BM6; (e) BM8; (f) BM10

strain energy of the crystal lattice when B atoms are further added. And during the solidification, the B atoms are discharged in front of the solid−liquid interface to reduce the strain energy, which facilitates the constitutional undercooling that is beneficial to the formation of dendrites.

The morphology of the dendrites in AlCoCrFeNiB$_x$ HEAs is sensitive to alloying contents. The interdendritic regions become larger obviously as B contents increase, and many precipitated phases, as indicated in Fig. 3, can be detected in interdendritic regions. The precipitated phases in the matrix, rich in Cr and B elements, belong to ordered intermetallics phases. From the XRD and EDS results (as shown in Table 1), the matrix of interdendrite is rich in Fe, Co and Cr elements. According to the previous research, regions rich in Fe, Co and Cr tend to form FCC solid-solution phases. And combined with the XRD analysis, the amount of FCC solid-solution phases increases with the addition of B. Therefore, the matrix structure in interdendritic regions is deduced to be FCC solid-solutions. When $x \leq 0.07$, the precipitates are mainly in particle-shape as seen in Figs. 3(b)−(e). When x exceeds 0.09, the "particles" assemble together, and form in stripe-shape, as seen in Fig. 3(f). The dendritic region is a mixture of rod-like and interlaced spinodal decomposition structures, marked by *DA* and *DB*, respectively.

With the addition of B element, distinct refinement of crystalline grain size occurs, such as sample BM0, 200−300 μm, sample BM4, 50−100 μm, until to sample BM10, 20−50 μm, as shown in Fig. 2.

3.3 Compressive properties

Figure 4 shows the compressive stress−strain curves of AlCoCrFeNiB$_x$ alloys with different B contents at the strain rate of 1.0×10^{-3} s^{-1}, and the compressive test results are listed in Table 2. The curve in Fig. 4 firstly

Table 1 Chemical compositions of $AlCoCrFeNiB_x$ HEAs

Alloy	Region	Mole fraction/%					
		Al	Co	Cr	Fe	Ni	B
BM0	Normal	20	20	20	20	20	0
	Part *A*	24.0	19.8	16.5	17.5	22.2	0
	Part *B*	1.1	19.1	46.9	28.2	4.7	0
BM1	Normal	19.96	19.96	19.96	19.96	19.96	0.20
	Part *DA*	26.4	18.6	15.8	16.7	22.5	0.0
	Part *DB*	23.9	18.8	17.9	18.4	20.9	0.0
	Interdendrite	15.3	13.7	41.2	15.0	14.8	0.0
BM2	Normal	19.92	19.92	19.92	19.92	19.92	0.40
	Part *DA*	15.3	13.7	41.3	15.0	14.8	0.0
	Part *DB*	15.3	13.7	41.3	15.0	14.8	0.0
	Interdendrite	11.8	15.2	13.7	41.3	15.0	0.0
BM3	Normal	19.88	19.88	19.88	19.88	19.88	0.60
	Part *DA*	23.7	18.7	18.1	19.1	20.4	0.0
	Part *DB*	21.4	19.6	20.4	19.3	19.3	0.0
	Interdendrite	4.1	5.4	23.9	7.3	4.6	54.7
BM4	Normal	19.84	19.84	19.84	19.84	19.84	0.80
	Part *DA*	27.5	18.3	14.3	16.1	23.8	0.0
	Part *DB*	21.0	18.6	21.1	20.2	19.1	0.0
	Precipitates	3.7	9.3	27.0	12.9	5.8	41.3
	Matrix	16.7	18.9	25.6	22.1	16.7	0.0
BM5	Normal	19.80	19.80	19.80	19.80	19.80	1.00
	Part *DA*	26.2	19.2	15.6	16.6	22.4	0.0
	Part *DB*	23.1	19.0	18.5	19.1	20.3	0.0
	Precipitates	5.8	11.8	17.4	14.8	8.2	42.0
	Matrix	12.9	18.7	32.9	24.7	10.8	0.0
BM6	Normal	19.76	19.76	19.76	19.76	19.76	1.20
	Part *DA*	28.0	18.7	14.4	16.5	22.4	0.0
	Part *DB*	22.6	19.0	18.8	19.4	20.2	0.0
	Precipitates	2.1	3.3	37.0	6.1	1.5	50.0
	Matrix	11.1	20.3	28.5	25.8	14.3	0.0
BM7	Normal	19.72	19.72	19.72	19.72	19.72	1.40
	Part *DA*	25.3	18.9	14.9	17.4	23.5	0.0
	Part *DB*	23.8	19.5	17.3	19.2	20.2	0.0
	Precipitates	8.2	8.1	21.7	9.5	8.5	44.0
	Matrix	13.0	19.8	29.9	25.5	11.8	0.0
BM8	Normal	19.68	19.68	19.68	19.68	19.68	1.60
	Part *DA*	27.4	18.6	13.5	16.3	24.2	0.0
	Part *DB*	24.6	18.8	16.4	18.6	21.6	0.0
	Precipitates	3.4	4.5	29.2	7.1	3.8	51.9
	Matrix	10.1	20.4	30.9	26.0	12.6	0.0
BM9	Normal	19.65	19.65	19.65	19.65	19.65	1.75
	Part *DA*	27.9	18.8	12.2	17.0	24.1	0.0
	Part *DB*	22.6	19.2	18.1	19.7	20.4	0.0
	Precipitates	3.0	5.3	27.4	9.0	3.3	52.0
	Matrix	15.2	19.3	26.8	23.9	14.8	0.0
BM10	Normal	19.61	19.61	19.61	19.61	19.61	1.95
	Part *DA*	30.5	17.9	11.2	15.4	25.0	0.0
	Part *DB*	22.9	19.4	18.1	19.5	20.1	0.0
	Precipitates	1.1	3.8	33.3	6.8	1.7	53.3
	Matrix	11.2	22.0	25.5	26.4	14.9	0.0

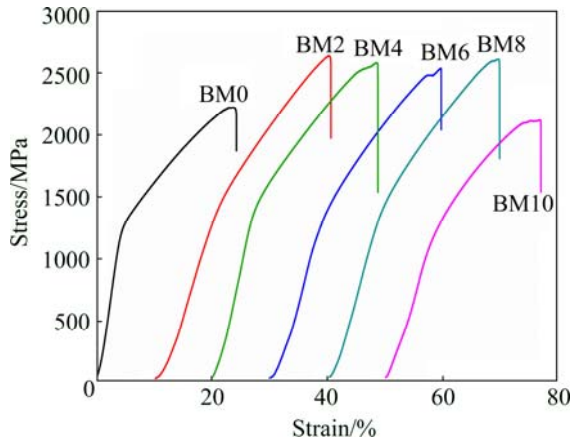

Fig. 4 Compressive properties of $AlCoCrFeNiB_x$ HEAs

shows a trend of increasing, and then declining. BM2 alloy exhibits the highest compression strength (2643.475 MPa), while from BM2 to BM8, the alloys show similar values (about 2600 MPa), subsequently drastically decrease to about 2100 MPa. As for the compression ratio, BM0 reveals a value of 24%. BM2−BM8 alloys show an increase (~30%), but afterwards, when x exceeds 0.08, the compression ratio declines to 27%, as shown in Table 2.

Table 2 Mechanical properties of $AlCoCrFeNiB_x$ alloy

Alloy	Compression strength/MPa	Yield strength/ MPa	Compression ratio/%
BM0	2227.0	1406.9	24.3
BM2	2643.5	1751.2	30.6
BM4	2586.7	1680.5	29.2
BM6	2543.0	1662.4	29.7
BM8	2619.5	1752.5	29.8
BM10	2121.0	1732.7	27.0

All of the tested samples exhibit typical intergranular fracture surface morphology. A small amount of B element segregates at crystal boundaries, which leads to the bonding strength of crystal boundaries much lower than that of internal regions of grains.

In this research, the compression strength of BM2 is higher than that of BM0, which can be due to the effect of B atomic solution strengthening in dendrites. According to the EDS results, B element cannot be detected neither in dendritic nor interdendritic regions of BM0−BM2, but can be detected in interdendritic regions of BM3−BM10. A conclusion can be obtained that the solid solubility of B atom in dendritic regions is rather small, between 0.4%−0.6% in mole fraction. As a result, when x exceeds 0.02, redundant B atoms are discharged from the dendrites. The FCC structural interdendritic region increases as B content increases, which enhances the plasticity, but is unfavorable to the compression strength improvement. However, as a result of further addition of B element, the formation of more and more (Cr,B)-rich intermetallic phases can improve the compression strength. And the similar compression strength (x= 0.02−0.08) may be due to the combined effects of the above two factors. The decrease of the compression strength ($x \geq 0.08$) is attributed to too much FCC phase.

3.4 Microhardness of $AlCoCrFeNiB_x$ HEAs

The microhardness of $AlCoCrFeNiB_x$ alloys is shown as Fig. 5. All of the $AlCoCrFeNiB_x$ HEAs possess high hardness. As B content increases from 0 to 0.1, the hardness firstly increases from HV 486.7 to HV 502.4, then, it declines to HV 460.7. Corresponding to the compressive test, the lattice distortion led by B element addition plays a dominating role in the hardness increase when x is in the range of 0−0.02. When x exceeds 0.02, the formation of more and more FCC phases could be the key reason for the decrease of the hardness. And this change is exactly consistent with the XRD and SEM analyses.

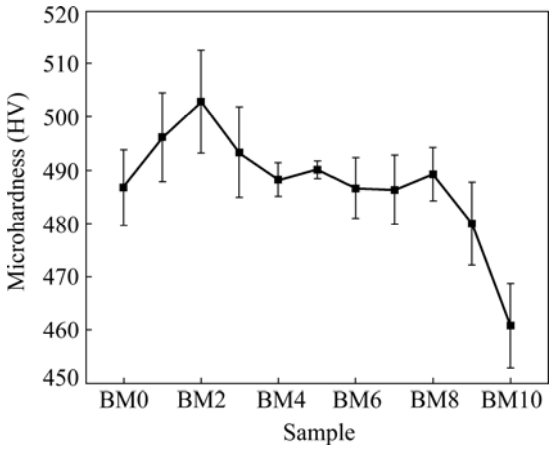

Fig. 5 Microhardness of $AlCoCrFeNiB_x$ HEAs

3.5 Magnetic properties

The magnetization curves of $AlCoCrFeNiB_x$ HEAs are shown in Fig. 6. Obviously, all of the alloys show typical ferromagnetic behavior. The specific saturation magnetizations of the alloys under the magnetic field of 3.98×10^3 A/m decrease from 53.91 to 43.75 $A\cdot m^2/kg$ with the increase of B contents. According to the following equation of the classification of magnetic properties [9]:

$$\chi = \frac{M}{H} = \frac{\sigma\rho}{4\pi H} \quad (1)$$

where χ is the permeability, M is the magnetization, H is the magnetic field intensity, σ is the specific saturation

magnetization, and ρ is the density of alloys. The decline of ferromagnetic behavior can be explained by the addition of the non-magnetic B element into the alloy system. Moreover, the coercive forces are 3664.5×10^3, 3358.9×10^3, ⋯, 3023.9×10^3 A/m when x=0, 0.02×10^3, ⋯, 0.1, respectively, which reveals better and better soft magnetic behavior. When the content of B element increases, all alloys still exhibit ferromagnetic property but the permeability shows little difference (5.6×10^{-3}−5.8×10^{-3}), according to Eq. (1).

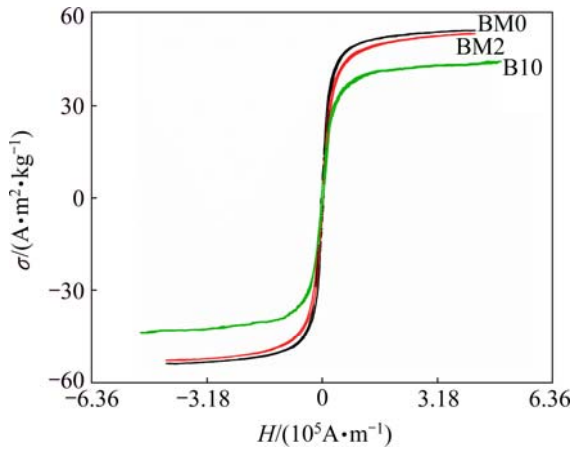

Fig. 6 Magnetization curves of $AlCoCrFeNiB_x$ HEAs

4 Conclusions

1) XRD and SEM results revealed that the crystal structures of $AlCoCrFeNiB_x$ alloys transformed from B2 + BCC to *B*2 + BCC + FCC structures with the addition of B element. The addition of B element facilitated the morphology changing from equiaxed grain to dendritic structure, accompanied with obvious refinement.

2) Both the fracture strength and compressive ratio exhibited a tendency of first increasing and then declining. When x=0.02, the values reached the highest value, 2643.475 MPa and 30.6%, respectively.

3) The hardness of the alloy exhibited a tendency of first increasing from HV 486.7 to HV 502.4, and then declining to HV 460.7 with the addition of B element.

4) With the increase of B element content, a decrease of coercive forces and the specific saturation magnetizations can be observed. And the decrease of coercive forces benefits the soft magnetic behavior.

References

[1] WANG Tong-min, FU Hong-wang, CHEN Zong-ning, XU Jun, ZHU Jing, GAO Fei, LI Ting-ju. A novel fading-resistant Al−3Ti−3B grain refiner for Al−Si alloys [J]. Journal of Alloys and Compounds, 2012, 511(1): 45−49.

[2] ZHANG Yu-bo, JIE Jin-chuan, WU Li, FU Ying, LI Mu, LU Yi-ping, LI Ting-ju. Microstructure and mechanical properties of Al−8 pct Si alloy prepared by direct chill casting under electromagnetic and ultrasonic fields [J]. Metallurgical and Materials Transactions A—Physical Metallurgy and Materials Science, 2014, 45(4): 2014−2022.

[3] CANTOR B, CHANG I T H, KNIGHT P, VINCENT A J B. Microstructural development in equiatomic multicomponent alloys [J]. Materials Science and Engineering A, 2004, 375−377: 213−218.

[4] YEH J W, CHEN S K, LIN S J, GAN J Y, CHIN T S, SHUN T T, TSAU C H, CHANG S Y. Nanostructured high–entropy alloys with multiple principle elements: Novel alloy design concept and outcomes [J]. Advanced Engineering Materials, 2004, 6(5): 299−303.

[5] ZHANG Y, ZUO T T, TANG Z, GAO M C, DAHMEN K A, LIAW P K, LU Z P. Microstructures and properties of high-entropy alloys [J]. Progress in Materials Science, 2014, 64: 1−93.

[6] LI Bao-yu, PENG Kun, HU Ai-ping, ZHOU Ling-ping, ZHU Jia-jun, LI De-yi. Structure and properties of $FeCoNiCrCu_{0.5}Al_x$ high entropy alloy [J]. Transactions Nonferrous Metals Society of China, 2013, 23(3): 735−741.

[7] WANG Z W, YUAN Y B, ZHENG R X, AMEYAMA K, MA C L. Microstructure and mechanical properties extruded 2024 aluminum alloy reinforced by $FeNiCoCrAl_3$ paticles [J]. Transactions Nonferrous Metals Society of China, 2014, 24(7): 2366−2373.

[8] NONG Zhi-sheng, ZHU Jing-chuan, YU Hai-ling, LAI Zhong-hong. First principles calculation of intermetallic compounds in FeTiCoNiVCrMnCuAl system high entropy alloy [J]. Transactions Nonferrous Metals Society of China, 2012, 22(6): 1437−1444.

[9] MA Sheng-guo, ZHANG Yong. Effect of Nb addition on the microstructure and properties of AlCoCrFeNi high-entropy alloy [J]. Materials Science and Engineering A, 2012, 532: 480−486.

[10] ZHU J M, FU H M, ZHANG H F, WANG A M, LI H, HU Z Q. Microstructure and compressive properties of multiprincipal component $AlCoCrFeNiC_x$ alloys [J]. Journal of Alloys and Compounds, 2011, 509(8): 3476−3480.

[11] DONG Yong, ZHOU Kai-yao, LU Yi-ping, GAO Xiao-xia, WANG Tong-min, LI Ting-ju. Effect of vanadium addition on the microstructure and properties of AlCoCrFeNi high entropy alloy [J]. Materials and Design, 2014, 57: 67−72.

[12] LI C, LI J C, ZHAO M, ZHANG L, JIANG Q. Microstructure and properties of $AlTiNiMnB_x$ high entropy alloys [J]. Materials Science and Technology, 2008, 24(3): 376−378.

[13] LEE C P, CHEN Y Y, HSU C Y, YEH J W, SHIH H C. The effect of boron on the corrosion resistance of the high entropy alloys $Al_{0.5}CoCrCuFeNiB_x$ [J]. Journal of the Eletrochemical Society, 2007, 154(8): C424−C430.

[14] BOERF R, ROOM R, MATTENS W C M. Cohesion in Metals [M]. Amsterdam: Amster Elsevier Science Publishing Company, 1989.

[15] HSU C Y, YEH J W, CHEN S K, SHUN T T. Wear resistance and high-temperature compression strength of FCC CuCoNiCrAl0.5Fe alloy with boron addition [J]. Metallurgical and Materials Transactions A, 2004, 35A(5): 1465−1469.

[16] XU Zhou, ZHAO Lian-cheng. Metal solid state phase transition principle [M]. Beijing: Science Press, 2004. (in Chinese)

[17] CHEN Zong-ning, WANG Tong-ming, GAO Lei, FU Hong-wang, LI Ting-ju. Grain refinement and tensile properties improvement of aluminum foundry alloys by inoculation with Al−B master alloy [J]. Materials Science and Engineering A, 2012, 553: 32−36.

[18] SHARMA P, ZHANG X, ZHANG Y, MAKINO A. Influence of microstructure on soft magnetic properties of low coreloss and high B-s Fe85Si2B8P4Cu1 nanocrystalline alloy [J]. Journal of Applied Physics, 2014, 115:1−3.

微量硼元素的添加对 AlCoCrFeNi 多主元合金显微组织和性能的影响

陈秋实，卢一平，董 勇，王同敏，李廷举

大连理工大学 材料科学与工程学院，大连 116024

摘 要：研究微量硼元素对 $AlCoCrFeNiB_x$(x = 0, 0.01, 0.02…0.09, 0.10, x 为摩尔分数)高熵合金微观组织和性能的影响。AlCoCrFeNi 高熵合金呈现典型的等轴晶结构，晶内伴随着明显的成分偏析。然而，随着硼元素的添加，合金呈现明显的树枝晶结构。在树枝晶内可以观察到典型的调幅分解结构。晶体结构也随着硼元素的增加由 B2 + BCC 结构转变为 B2 + BCC + FCC 的混合结构；合金硬度呈先升后降趋势，由 HV 486.7 升高至 HV 502.4，最后降低至 HV 460.7；压缩断裂强度在 x=0.08 前呈上升趋势，之后呈下降趋势；合金呈软磁性，其矫顽力和饱和磁化强度均随着硼元素含量增加而下降，表明硼元素对合金软磁性有提高作用。

关键词：高熵合金；硼元素；显微组织；压缩强度；硬度；磁性能

(Edited by Yun-bin HE)